

Dynamics of Charge-Density-Wave *puddles* in $2H\text{-NbSe}_2$

Shreya Kumbhakar^{1,2,*}, Marina Esposito^{1,3,*}, Anjan Kumar N M^{1,*}, Tommaso Confolone^{1,4}, Liwen Feng¹, Rafiqul Alam², Flavia Lo Sardo^{2,5}, Davide Masarotti⁶, Francesco Tafuri³, Thomas Böhm², Mahmoud Abdel-Hafiez⁷, Sushmita Chandra⁸, Claudia Felser⁸, Kornelius Nielsch^{2,5}, Nicola Poccia^{1,3,†}, Stefan Kaiser^{1,†}, and Golam Haider^{2,†}

¹*Institute of Solid State and Materials Physics, University of Technology, Dresden, Germany*

²*Leibniz Institute for Solid State and Materials Research Dresden (IFW Dresden) Dresden 01069, Germany*

³*Department of Physics, University of Naples Federico II, Naples 80126, Italy*

⁴*Institute of Applied Physics Technische Universität Dresden 01062 Dresden, Germany*

⁵*Institute of Materials Science Technische Universität Dresden 01062 Dresden, Germany*

⁶*Department of Electrical Engineering and Information Technology,*

University of Naples Federico II, Naples I-80126, Italy

⁷*Department of Applied Physics and Astronomy, University of Sharjah, United Arab Emirates*

⁸*Max Planck Institute for Chemical Physics of Solids, 01187 Dresden, Germany*

** equal contribution and*

† g.haider@ifw-dresden.de, stefan.kaiser@tu-dresden.de, nicola.poccia@unina.it

Electronic phases in quantum materials are often governed by nanoscale inhomogeneity, where local order develops within spatially confined regions or *puddles*. A prominent example is an incommensurate charge-density-wave (I-CDW) that comprises locally commensurate domains. In $2H\text{-NbSe}_2$, such an I-CDW state persists alongside lattice anharmonicity and superconductivity, raising fundamental questions about the dynamical stabilization of CDW order in puddles. Here, we probe the puddle-dynamics in $2H\text{-NbSe}_2$. Raman scattering reveals a strong Fano-coupling between the interlayer shear vibration and the CDW amplitude mode. Time-resolved reflectivity measurement shows a low-frequency ~ 0.15 THz coherent overdamped oscillation onsetting within the CDW regime at ~ 17 K, pointing towards a so far unexplored transition. This we identify as a Fano-coupled phonon-CDW hybrid emerging from the collective dynamics of CDW puddles. These dynamics highlight how lattice pinning and electronic correlations in layered materials affect the CDW order, which is crucial for the design of novel van der Waals devices.

Strongly correlated electron systems, in which lattice, charge, spin, and orbital degrees of freedom interact actively with each other, naturally develop local inhomogeneities or ‘*puddles*’ of distinct types of order [1–12], driven by the competition of different phases [13, 14]. Recent experiments [15–17] suggest that the coexistence of these puddles can generate a multiband or multigap system [16, 18], where new interference effects emerge from a generalized ‘Fano’ coupling [19] between the different bands. Importantly, such systems, ranging from ultracold gases to high- T_c cuprates [20–26], can be tuned close to a Fano resonance condition through doping, external pressure, internal chemical pressure or ‘microstrain’ in layered materials, magnetic fields, or geometrical control [16, 17, 27–29], where particle–particle correlations and scattering intensities are strongly enhanced. Here, we investigate $2H\text{-NbSe}_2$, a prominent system where both superconductivity (SC) and unconventional CDW phases coexist at low temperatures [30–36]. The CDW phase comprises puddles of distinct local CDW commensurations [7, 37, 38]. We study the temporal dynamics of the puddles, which remain elusive despite extensive investigation of their spatial distribution [7, 37–39]. The simpler chemical structure of NbSe_2 among materials with complexity [3] helps in disentangling the CDW-puddle dynamics from other intertwined orders [15, 35, 40, 41], making it a suitable material choice.

The puddle-dynamics can provide unique insights into the formation of the CDW order itself. For example,

although phonons soften strongly near the CDW wave vector in NbSe_2 [34, 42], it remains debated whether phonons alone drive the transition or whether electronic correlations play an essential role. One of the primary anomalies causing this debate is the persistence of CDW-like spectral features above T_{CDW} before the onset of phonon-softening or in the absence of substantial lattice distortions. The microscopic character of the pronounced short-range CDW order observed well above T_{CDW} [31, 38, 39, 43] remains unclear *i.e.* whether they represent amplitude vs. phase incoherence, domain dynamics, or preformed electronic order. The very nature of CDW in NbSe_2 is also not understood clearly as to why the CDW wave vector does not coincide with a strong nesting feature of the Fermi surface [44, 45] and is not perfectly commensurate, raising the question of how anharmonic lattice effects [34, 42], momentum- and orbital-dependent electron-phonon coupling [45], and higher-order free-energy terms stabilize a particular triangular pattern of the CDW domains [7, 46, 47].

In this study, we perform Raman scattering and ultrafast spectroscopy measurements on bulk-like mechanically exfoliated flakes of $2H\text{-NbSe}_2$. We find that the CDW amplitude mode exhibits a strong Fano lineshape that captures the coupling between the interlayer shear mode and the CDW mode. Time-resolved reflectivity of the crystals reveals an overdamped oscillation that is intertwined with the electronic response, tracking both CDW and SC orders, setting in at $T_{\text{CDW}} \sim 28$ K and

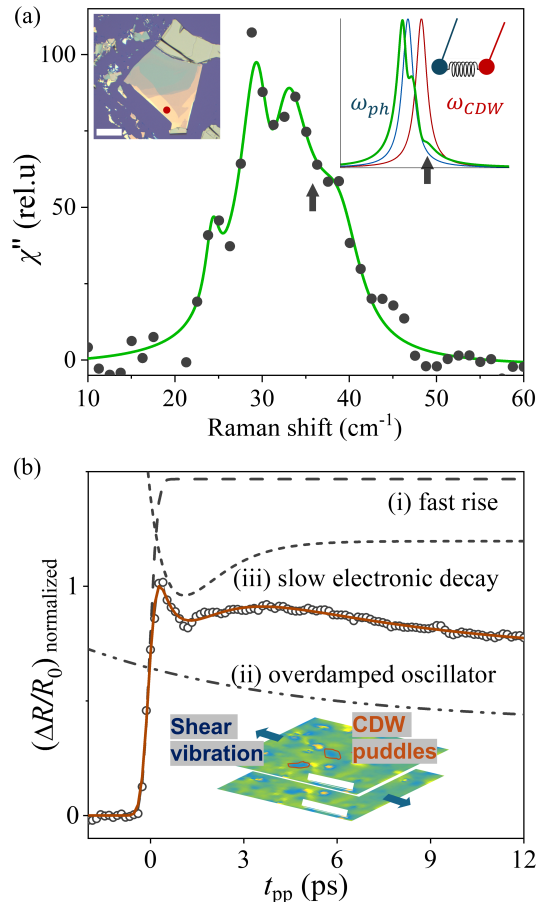


FIG. 1. Fano-coupled phonon-CDW response. (a) Raman susceptibility, χ'' measured in unpolarized backscattering configuration on a mechanically exfoliated bulk-flake (thickness ~ 60 nm) of NbSe₂ on Si/SiO₂ substrate at 14 K is shown. The arrow points to a broad shoulder at ~ 40 cm⁻¹. The green solid line shows a fit to the data using a Fano resonance model, as sketched in the right inset of Fig. 1a. Left inset: Optical image of the flake of NbSe₂, with the red dot pointing the point of Raman measurements. Right inset: Fano coupling between two discrete oscillators, modelled by Lorentzian lineshapes (blue and red solid curves), leads to the Breit-Wigner Fano lineshape (green solid line). The black arrow represents the shoulder, which is analogous to the data in (a). (b) Time-resolved reflectivity change ($\Delta R/R_0$), normalized with respect to its peak value, of NbSe₂ single crystals measured at $T \sim 2$ K with $40 \mu\text{J}/\text{cm}^2$ of 1.2 eV pump fluence is shown. R_0 is the reflectivity at zero pump-probe time delay (t_{pp}). The data is fitted by a convolution of three distinct components, which are shown separately by the dashed, dotted, and dashed-dotted lines, respectively and discussed further in the main text. (Inset:) The schematic depicts CDW puddles (represented by regions marked with red solid lines). The blue arrows indicate the interlayer shear vibration that couples with the CDW. The colour maps in the square sheets, indicating the layers, are CDW modulations measured via STM experiments reproduced from Ref. [37].

$T_c \sim 7$ K, respectively. The divergence of the electron

relaxation time in the ultrafast response, together with the low-frequency of the oscillation at $\sim 14 - 17$ K within the CDW phase, establishes an onset of a coherent collective dynamics of the CDW-puddles, which is *glassy* in nature. A correlation between the Fano coupling parameter and the oscillation frequency suggests that a competition between different CDW commensuration orders and an early onset of SC fluctuations is reflected in the puddle dynamics.

Figure 1(a) shows the unpolarized Raman susceptibility, χ'' , measured in bulk flakes of NbSe₂ mechanically exfoliated inside a glovebox and loaded in-situ for environment-protected Raman measurements. (See left inset of Fig. 1a and Materials and Methods for more details). We focus on the low-frequency spectral region up to 60 cm⁻¹. We observe a peak at 29 cm⁻¹, corresponding to the interlayer shear vibration [48] and another peak at 35 cm⁻¹, at which the CDW amplitude mode [49–52] has been reported. The arrow in the figure indicates a broad shoulder at 40 cm⁻¹. There is also a prominent notch at 25 cm⁻¹. These features reveal a coupling between the interlayer phonon and the CDW order that is accurately described by a Fano lineshape (green solid line) [53–55], sketched in the right inset of Fig. 1(a). (See Materials and Methods for discussion.) Such a Fano coupling is intimately connected to the presence of puddles of local order in the system [15–18], in this case, the CDW puddles [7, 37, 38], motivating us to investigate its dynamics. Fig 1(b) shows the time-resolved ultrafast optical reflectivity changes, $\Delta R/R_0$ at 2 K in single crystals of NbSe₂. (See Materials and Methods for details on the pump-probe experiments.) We observe and accurately model the response as a convolution of (i) a fast rise in $\Delta R/R_0$ close to zero pump-probe delay ($t_{pp} = 0$), followed by (ii) an overdamped oscillation before approaching (iii) a slow decay (See Materials and Methods for discussion on the fitting.) We find this overdamped oscillation has a low-frequency ~ 0.18 THz, compared to the CDW amplitude mode ~ 1.2 THz [50, 51, 56, 57]. In the following, we are going to identify this as a new collective mode in the system emerging from the CDW puddles.

In Fig. 2(a), we show the T -dependent ultrafast response in NbSe₂ from 100 K down to 2 K (see Supporting Information SI Sec I for detailed T -dependence). We observe a noticeable drop in the overall amplitude of the $\Delta R/R_0$ above $T_c \sim 6 - 7$ K, and even more significant reduction above ~ 13.7 K. Furthermore, above 17 K, $\Delta R/R_0$ changes sign. We will show in further analysis that 17 K is also the temperature below which the overdamped oscillation (discussed in Fig. 1(b)) sets in. The largest negative response in $\Delta R/R_0$ is reached close to $T_{\text{CDW}} \sim 28$ K. The transition temperatures for SC and CDW, T_c and T_{CDW} , respectively have been extracted from the transport characterization in Fig 2(b), with blue and beige-shaded regions marking the corresponding phases in Fig. 2(b)-2(e). These changes in the ultrafast response have been quantitatively captured by

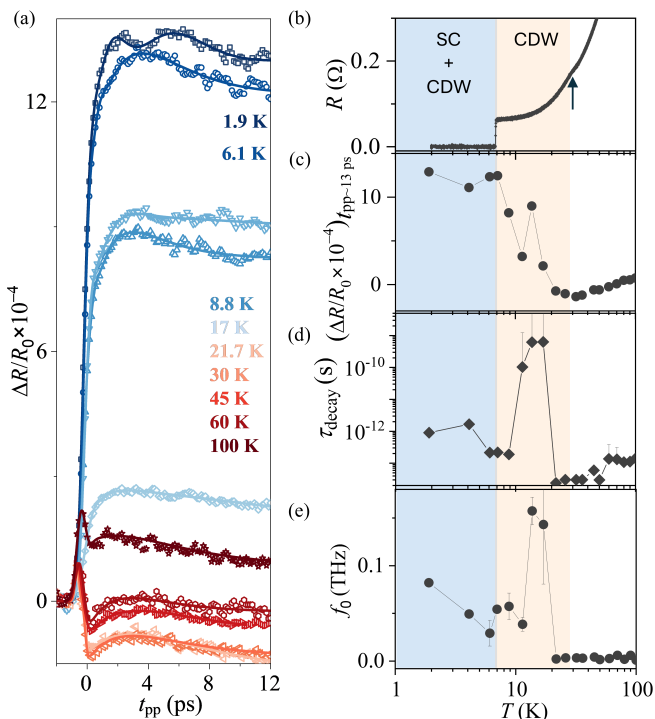


FIG. 2. **Temperature-dependent ultrafast dynamics in bulk NbSe₂:** (a) The time-resolved reflectivity, $\Delta R/R_0$ is shown at different temperatures (T s) from 1.9 K–100 K. The open points are the measured data and the solid lines are the respective fits using the model discussed in Fig. 1(b). (b) Representative T -dependent four-probe resistance, R of the NbSe₂ crystals is shown. R jumps to nearly zero resistance (≈ 1 n Ω) at $T_c \sim 7$ K, indicating the superconducting transition. The data shows a kink at the CDW transition temperature, $T_{CDW} \sim 28$ K, marked by the solid arrow. The blue and beige regions are marked based on these transition temperatures. (c)–(e) show the T -dependence of the long-lived reflectivity, *i.e.* $\Delta R/R_0$ at $t_{pp} \sim 13$ ps, the relaxation time, τ_{decay} , and overdamped oscillation frequency, f_0 , estimated from the fits, respectively.

the long-lived reflectivity change, $\Delta R/R_0$ at $t_{pp} \sim 13$ ps, as shown in Fig. 2(c). Analyzing $\Delta R/R_0$ of Fig. 2(a) with the model discussed in Fig. 1(b) (See Eq. [2] in Materials and Methods), Fig 2(d), and (e) show the oscillation frequency (f_0), and the decay time (τ_{decay}), respectively.

τ_{decay} (in Fig. 2(d)) shows a significant increase first at 14 K, and then another rise at T_c . The divergence of τ_{decay} is generally connected to a quasiparticle recombination bottleneck effect (e.g., Rothwarf–Taylor bottleneck) associated with gap opening, or from critical slowing down of collective order parameter dynamics near the phase transition [58, 59]. The increase in τ_{decay} close to T_c is consistent with the opening of a SC gap [58, 60, 61]. However, the significant enhancement of τ_{decay} at 14–17 K has not been discussed before. Interestingly, τ_{decay} has no sharp change at T_{CDW} , similar to previous report [36]. This is probably because the CDW gap has been observed to be present until room T , though inco-

herent in nature [43], with the coherence setting in only at T_{CDW} [31]. On the other hand, the diverging behavior of τ_{decay} at 14–17 K, where no electronic gap opening has been reported, implies a critical slowing down of electrons from the onset of a glassy dynamics.

We observe f_0 (in Fig. 2(e)) to be nearly zero above 17 K. At 17 K, it increases sharply to ~ 0.15 THz, staying almost constant until 14 K. Below 14 K, we again observe a softening of f_0 , down to ~ 0.1 THz. Its value remains almost constant until 7 K, close to T_c , below which it shows a monotonic increase. The softening of f_0 to almost zero at higher T s indicates that the oscillation does not emerge from a simple phononic mode (like coherent phonons), but rather a *new* collective order in the system, which in this case is the CDW order. The low-frequency of the oscillation (~ 0.15 THz) further indicates that this is not driven purely by the (fast) CDW amplitude mode (at 40 cm⁻¹ $\simeq 1.2$ THz) but rather by the (slower) fluctuations of CDW puddles.

We make two key observations here. Firstly, the coherent oscillations set in at 17 K, in the same T -window as τ_{decay} diverges, supporting the onset of a *glassy* dynamics of CDW-puddles. Glassy dynamics often appear from electronic frustration and/or disorder [62]. In this case, we believe a strong competition between different CDW commensurations promotes this [63–65]. Secondly, the frequency softens again at 14 K (to ~ 0.1 THz) and increases monotonically below T_c . This softening may be related to the onset of SC fluctuations above T_c that affect the puddle dynamics [5, 52, 66, 67].

To further characterize this complex interplay of phases, we have carried out T -dependent Raman measurements, as shown in Fig. 3a. (See SI Sec III for detailed T -dependence.) First, we observe a noticeable reduction in the overall intensity of the spectra above 17 K. This is quantitatively captured by the T -dependence of χ'' at 29 cm⁻¹ and 35 cm⁻¹ (associated with the interlayer shear vibration and CDW amplitude modes respectively) shown in the inset. Second, the features at 35 cm⁻¹ and 40 cm⁻¹, which we attribute to a ph-CDW Fano coupling effect (discussed in Fig. 1(a)), have non-trivial T -dependences. Although a peak at 35 cm⁻¹ can be identified until 100 K, the broad shoulder centred at 40 cm⁻¹, can be clearly resolved only at lower temperatures (below $T \sim 50$ K as we show later). We also note from the inset nearly constant magnitudes of χ'' with decreasing T below $T \sim 50$ K until 17 K, indicating changes in the Fano coupling behaviour at these temperatures. To better understand this, we plot the Raman spectra at two representative temperatures, $T \sim 94$ K and 32 K in the top and bottom panels of Fig. 3(b). At $T \sim 94$ K, the contribution from three distinct Lorentzians captures the data accurately. We note the persistence of the peak at 35 cm⁻¹ above T_{CDW} is consistent with the observation of the CDW gap even until higher T s [43]. Furthermore, we believe that the peak at 25 cm⁻¹ is a splitting (of ≈ 4 cm⁻¹) from the doubly degenerate E_{2g} peak at 29 cm⁻¹ of the interlayer shear vibration due to strain

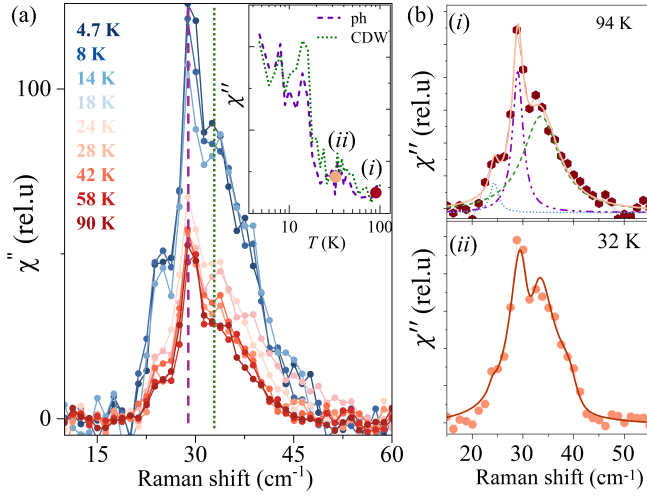


FIG. 3. **Temperature dependence of the Raman susceptibility of bulk NbSe₂.** (a) Raman susceptibility (χ'') is measured at different T s on bulk flakes of NbSe₂. The inset plots the value of χ'' at the frequencies marked by the dashed and dotted lines. (b) χ'' is plotted at three distinct $T \sim 24, 32,$ and 100 K. The solid lines represent fits to the data. At 100 K, the data is fitted with additive contributions from three distinct Lorentzian lineshapes, depicted by the dashed lines, which represent the interlayer shear phonon peak at ~ 29 cm⁻¹, CDW amplitude mode at ~ 35 cm⁻¹, and another peak at 25 cm⁻¹, that is identified with a split E_{2g} peak of the interlayer shear vibration. The data at 32 K is fitted by a Fano lineshape, as we discuss further in the text.

induced from CDW fluctuations and is hence intimately tied to the CDW amplitude mode. Though a splitting of E_{2g} peaks from strain has been experimentally and theoretically measured in intercalated NbSe₂ layers from strain [68], the same has not been observed on bulk 2H-NbSe₂ layers. At lower temperatures (e.g., at 32 K in the bottom panel of Fig. 3(b)), we clearly observe the presence of a broad shoulder at 40 cm⁻¹, that is accurately modelled by a Fano resonance between the phonon and CDW amplitude modes (See Materials and Methods for fit details).

Figure 4 plots the T -dependence of the Fano coupling parameter, ν , extracted from the Raman response along with f_0 . We find a strong fluctuating onset below 50 K, that starts showing a monotonic increase below $T_{\text{CDW}} \sim 28$ K. (SI Sec VI and V shows the rise time and amplitude of the ultrafast response and a shoulder close to the out-of-plane vibration E_{2g} peak at ~ 240 cm⁻¹ with similar T -dependence, respectively.) At 17 K, ν reaches a maximum value, below which it decreases again, yielding a stable plateau from ~ 14 K onwards to the lowest measurable temperatures. We note that these temperatures do not manifest in the phase characterization from transport (shown by blue and beige regions). Thus, our data capture transitions marking the onset of novel dynamics. (See SI Sec VI for specific heat characterization for further support.) The Fano coupling is intimately related

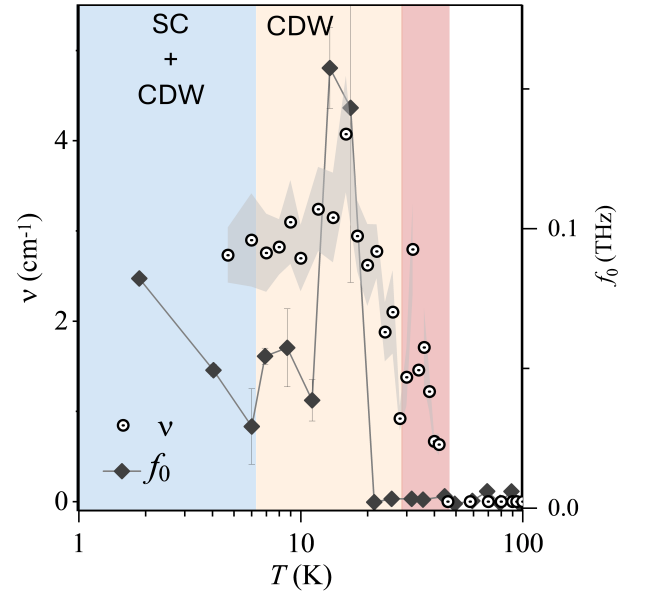


FIG. 4. **Temperature-dependence of the Fano coupling factor ν ,** estimated from the fits of the Raman susceptibility, χ'' at different T s is plotted on the left-axis. The grey-shaded region represents the fitting error. The right-axis plots the overdamped oscillation frequency, f_0 , obtained from the ultrafast response. Blue and beige shaded regions are marked based on the superconducting and CDW transition temperatures, characterized from electrical transport in Fig. 2(a). The red region marks, the onset of ν as discussed further in the text.

to phase-separation or phase-coexistence in a system [16–18], which in this case is the CDW puddles. From the onset of ν below 50 K, we conclude an *incoherent* puddle regime begins at this temperature, that is well-above T_{CDW} , marked by the red shaded region. A collective coherent motion only sets in at 17 K, captured by the increase of f_0 where ν attains its maximum strength likely from the competing CDW orders. This indicates that local response from the puddles, represented by ν , captures the emerging glassy collective dynamics at ~ 17 K. With further decrease in T , ν stabilizes below ~ 14 K where f_0 decreases as well. We could interpret this as a possible onset of SC above T_c (as also proposed in [52]), that impacts the CDW order and commensuration and is thus manifested in the puddle dynamics.

In summary, both ultrafast and Raman measurements reveal the onset of a new dynamics in 2H-NbSe₂ that is driven by the local CDW domains, or puddles. Locally, this manifests as a Fano coupling between the interlayer shear vibration and CDW amplitude mode in the Raman spectra, which directly corroborates the dynamics measured in the ultrafast response. Such a coupling sheds insight into multiple longstanding questions about the CDW phase in NbSe₂. First, it explains why CDW amplitude mode oscillations corresponding to 40 cm⁻¹ could not be clearly observed in the ultrafast response before. Second, it suggests an en-

hanced coherence of the CDW phase with decreasing interlayer shear strain, providing a possible route for significant enhancement in T_{CDW} from the bulk to the monolayer [69]. Third, the Fano coupling can aid in CDW incommensuration in NbSe₂, which remains an open question [34, 42, 44, 45]. Fourth, the microscopic fluctuations observed above T_{CDW} [31, 38, 39, 43] likely represent preformed electronic order and phase incoherence, as we see signatures of the CDW amplitude mode even until 100 K. Our results establish how local dynamics in puddles shapes the global response in a material. This can be used as a recipe to engineer novel functionalities in quantum materials.

I. MATERIAL AND METHODS

A. Material growth

High-quality single crystals of 2H-NbSe₂ were grown using the conventional chemical vapour transport (CVT) method. Initially, stoichiometric amounts of niobium powder (Alfa Aesar, 99.99%) and selenium powder (Sigma-Aldrich, 99.98%) were thoroughly mixed and sealed under vacuum in a quartz ampoule with iodine ($\sim 3 \text{ mg}\cdot\text{cm}^{-3}$) as the transport agent. The sealed ampoule was placed in a dual-zone furnace with a temperature gradient of 800° C (source zone) and 720° C (growth zone) and maintained for a period of 15 days. After slowly cooling to room temperature, shiny layered NbSe₂ single crystals with typical lateral dimensions of a few millimeters were obtained.

B. Raman Measurements

Raman measurements were carried out in a polarized backscattering configuration using a WITec Alpha 300 confocal Raman microscope equipped with a 50× objective (NA = 0.9), enabling a spot size of 1 micron with a continuous-wave 532 nm laser.

High spectral resolution was achieved using a diffraction grating with 1800 lines mm^{-1} , providing a resolution of approximately 1.2 cm^{-1} . A 532 nm RayShield filter enabled the detection of low-frequency Raman modes down to 10 cm^{-1} on both the Stokes and anti-Stokes sides of the spectrum. The laser power at the sample was monitored with a calibrated power meter and set to 1 mW for single-point spectra. This power was confirmed not to induce damage or degradation of the flakes during acquisition (60 s per spectrum, averaging over 10 accumulations). Cryogenic measurements from 300 K to 4 K were carried out using a continuous flow cryostat Microstat HiRes from Oxford Instruments.

NbSe₂ flakes were exfoliated from the single crystals, grown as discussed above, on cleaned Si/SiO₂ substrates inside an Argon-filled glovebox and loaded in-situ in the

cryostat for Raman measurements. This ensured pristine surfaces of the flakes protected from environmental degradation.

C. Ultrafast measurements

We performed femtosecond nondegenerate pump-probe reflectivity measurements on high-quality single crystals. The ultrafast experiments used 190 fs laser pulses in a reflection setup, with a 1030 nm pump beam and a 680 nm probe beam. The laser pulses were generated by a regenerative amplifier system (Pharos, Light Conversion; 1030 nm central wavelength, 10 kHz repetition rate, 190 fs pulse duration). The output beam was split into two parts. One part was sent to an optical parametric amplifier to produce the 680 nm probe beam, while the 1030 nm beam was used as the pump to excite the sample.

The pump and probe beams were linearly polarized and set perpendicular to each other to reduce coherent artifacts and polarization-related interference effects. The time delay between the pump and probe pulses was controlled using a motorized delay stage. The pump beam was modulated with a mechanical chopper. The resulting pump-induced change in reflectivity ($\Delta R/R_0$) was measured using a photodiode and lock-in detection for improved signal sensitivity.

Temperature-dependent measurements were performed in a continuous-flow helium cryostat (Optistat CF, Oxford Instruments), which provided an inert environment and maintained a clean sample surface during the experiment. The full-width at half maximum (FWHM) spot sizes were about 200 μm for the pump and 100 μm for the probe, ensuring uniform excitation within the measured area. The pump and was kept constant at 40 $\mu\text{J}/\text{cm}^2$ (that is below the threshold of $\sim 1 \text{ mJ}/\text{cm}^2$ for the suppression of the CDW state [36, 70, 71]), and 20 $\mu\text{J}/\text{cm}^2$, respectively, for all temperatures studied in Fig. 2.

D. Fano lineshape analysis of the Raman response

The experimentally measured Raman spectra have been multiplied by the Bose factor [72] to calculate the Raman susceptibility after subtracting a smooth background. The spectra have been then fitted with a Fano lineshape [55, 73–76], captured by the following expression:

$$f(\omega) \sim \frac{\pi r(\omega)[((\omega - \omega_{CDW}) + \nu\eta)^2 + \gamma_{CDW}(\nu^2\pi r(\omega) + \gamma_{CDW})]}{(\omega - \omega_{CDW} - \nu^2 R(\omega))^2 + (\nu^2\pi r(\omega) + \gamma_{CDW})^2} + \frac{\gamma_{CDW}^2(\nu R(\omega) + \eta)^2}{(\omega - \omega_{CDW} - \nu^2 R(\omega))^2 + (\nu^2\pi r(\omega) + \gamma_{CDW})^2}.$$

where:

$$r(\omega) = \frac{\gamma_{ph}^2}{(\omega - \omega_{ph})^2 + \gamma_{ph}^2}$$

and $R(\omega)$ is derived as Hilbert transform of $r(\omega)$. Here, ω is the Raman-frequency shift. $\omega_{ph}, \omega_{CDW}$ are the centre frequencies, $\gamma_{ph}, \gamma_{CDW}$ are the intrinsic dampings of the oscillators corresponding to the interlayer shear phonon and the CDW amplitude modes, respectively. $\eta = A_{CDW}/A_{ph}$ defines the ratio of the Raman amplitudes of the two Raman scattering channels. ν characterizes the coupling strength between the two modes. See SI Sec IV for further discussion of the Fano lineshape analysis.

E. Analysis of the pump-probe response

We have implemented a convolution of fast rise, slow decay and overdamped oscillator to fit the transient time-resolved reflectivity as follows.

$$\frac{\Delta R}{R_0} = A(\text{erf}(\frac{t-t_0}{t_{rise}}) + 1) * (\exp(-\frac{t}{\tau_{decay}}) + B) \quad (1)$$

$$* (\exp(-\gamma t) \cos(2\pi f t + \phi) + C) \quad (2)$$

t_0 and t_{rise} are respectively the onset and rise time of the ultrafast response.

τ_{decay} represents the relaxation time of the decay dynamics. B is an offset to the decay, which physically represents a heating term.

f is the frequency of the overdamped oscillation, and C is an offset to the damping. The intrinsic frequency of oscillation, f_0 is $f = \sqrt{f_0^2 + \gamma^2}$, where γ is the damping factor.

II. AUTHOR CONTRIBUTIONS

S.K., M.E. and A.K.N.M. contributed equally to this work. G.H., S.Ka. and N.P. conceived and designed the experiments. S.K. and A.K.N.M performed the ultrafast measurements with help from L.F., and analyzed the data. S.K., and M.E. performed the Raman measurements with support from T.C., R. A., F.L.S., and performed the subsequent analysis. S.K., M.E., and T.B discussed the acquisition and analysis of the Raman spectra. The crystals were provided by S.C. and C.F.. M. A-H performed the specific heat measurements that provided additional support to the data. D. M., F.T., M. A-H, and K. N. validated and discussed the results with G.H., S.Ka. and N.P. S. K., G.H., S.Ka., and N.P. wrote the manuscript. All authors discussed the manuscript.

III. ACKNOWLEDGEMENTS

N.P. acknowledges the partial funding by the European Union (ERC-CoG, 3DCuT, 101124606), by the Funded by the Deutsche Forschungsgemeinschaft (DFG, German Research Foundation): DFG 460444718, DFG 512734967, DFG 452128813, DFG 539383397. G.H. acknowledges financial support through start-up funding from IFW Dresden. We acknowledge support from the Deutsche Forschungsgemeinschaft (DFG) through the Würzburg-Dresden Cluster of Excellence on Complexity, Topology and Dynamics in Quantum Matter—ctd.qmat (EXC 2147, Project No. 390858490) and Deutsche Forschungsgemeinschaft (DFG), SFB 1143 (project id 247310070). S.Ka. acknowledges funding by the European Union (ERC, T-Higgs, GA 101044657). (Views and opinions expressed are however, those of the author(s) only and do not necessarily reflect those of the European Union or the European Research Council Executive Agency. Neither the European Union nor the granting authority can be held responsible for them). F.T. and D. M. would like to acknowledge the PNRR MUR Project PE0000023 NQSTI. The authors thank Dr. Amit Pawabke for valuable discussions and insights. G.H. gratefully acknowledges the support from Dr. Matthias Finger of Oxford Instruments (WITec).

-
- [1] Dagotto, E. Complexity in Strongly Correlated Electronic Systems. *Science* **2005**, *309*, 257–262.
- [2] Qazilbash, M. M.; Brehm, M.; Chae, B.-G.; Ho, P.-C.; Andreev, G. O.; Kim, B.-J.; Yun, S. J.; Balatsky, A. V.; Maple, M. B.; Keilmann, F.; Kim, H.-T.; Basov, D. N. Mott Transition in VO₂ Revealed by Infrared Spectroscopy and Nano-Imaging. *Science* **2007**, *318*, 1750–1753.
- [3] Dagotto, E. Nanoscale Phase Separation and Colossal Magnetoresistance, Springer-Verlag, Berlin. **2002**,
- [4] Ricci, A.; Poccia, N.; Campi, G.; Joseph, B.; Arrighetti, G.; Barba, L.; Reynolds, M.; Burghammer, M.; Takeya, H.; Mizuguchi, Y.; Takano, Y.; Colapietro, M.; Saini, N. L.; Bianconi, A. Nanoscale phase separation in the iron chalcogenide superconductor K_{0.8}Fe_{1.6}Se₂ as seen via scanning nanofocused x-ray diffraction. *Phys. Rev. B* **2011**, *84*, 060511.
- [5] Joe, Y. I.; Chen, X.; Ghaemi, P.; Finkelstein, K.; de La Peña, G.; Gan, Y.; Lee, J.; Yuan, S.; Geck, J.; MacDougall, G.; others Emergence of charge density wave domain walls above the superconducting dome in 1 T-TiSe₂. *Nat. Phys.* **2014**, *10*, 421–425.
- [6] Sajan, S.; Guo, H.; Agarwal, T.; Sánchez-Ramírez, I.; Patra, C.; Vergniory, M. G.; de Juan, F.; Singh, R. P.; M. Ugeda, M. Atomic-scale mapping of superconductivity in the incoherent CDW mosaic phase of a transition

- metal dichalcogenide. *Nano Lett.* **2025**, *25*, 6654–6660.
- [7] Yoshizawa, S.; Sagisaka, K.; Sakata, H. Visualization of Alternating Triangular Domains of Charge Density Waves in $2H\text{-NbSe}_2$ by Scanning Tunneling Microscopy. *Phys. Rev. Lett.* **2024**, *132*, 056401.
- [8] Bianconi, A.; Saini, N. L.; Lanzara, A.; Missori, M.; Rossetti, T.; Oyanagi, H.; Yamaguchi, H.; Oka, K.; Ito, T. Determination of the Local Lattice Distortions in the CuO_2 Plane of $\text{La}_{1.85}\text{Sr}_{0.15}\text{CuO}_4$. *Phys. Rev. Lett.* **1996**, *76*, 3412–3415.
- [9] Bianconi, A.; Lusignoli, M.; Saini, N. L.; Bordet, P.; Kvik, Å.; Radaelli, P. Stripe structure of the CuO 2 plane in $\text{Bi}_2\text{Sr}_2\text{CaCu}_2\text{O}_{8+y}$ by anomalous X-ray diffraction. *Phys. Rev. B.* **1996**, *54*, 4310.
- [10] Poccia, N.; Ricci, A.; Campi, G.; Fratini, M.; Puri, A.; Gioacchino, D. D.; Marcelli, A.; Reynolds, M.; Burghammer, M.; Saini, N. L.; others Optimum inhomogeneity of local lattice distortions in $\text{La}_2\text{CuO}_{4+y}$. *Proc. Natl. Acad. Sci. U. S. A.* **2012**, *109*, 15685–15690.
- [11] Fratini, M.; Poccia, N.; Ricci, A.; Campi, G.; Burghammer, M.; Aeppli, G.; Bianconi, A. Scale-free structural organization of oxygen interstitials in $\text{La}_2\text{CuO}_{4+y}$. *Nature* **2010**, *466*, 841–844.
- [12] Campi, G.; Bianconi, A.; Poccia, N.; Bianconi, G.; Barba, L.; Arrighetti, G.; Innocenti, D.; Karpinski, J.; Zhigadlo, N. D.; Kazakov, S. M.; others Inhomogeneity of charge-density-wave order and quenched disorder in a high- T_c superconductor. *Nature* **2015**, *525*, 359–362.
- [13] Emery, V.; Kivelson, S.; Lin, H. Phase separation in the t - J model. *Phys. Rev. Lett.* **1990**, *64*, 475.
- [14] Kivelson, S. A.; Fradkin, E.; Emery, V. J. Electronic liquid-crystal phases of a doped Mott insulator. *Nature* **1998**, *393*, 550–553.
- [15] Chu, H.; Kovalev, S.; Wang, Z. X.; Schwarz, L.; Dong, T.; Feng, L.; Haenel, R.; Kim, M.-J.; Shabestari, P.; Hoang, L. P.; others Fano interference between collective modes in cuprate high- T_c superconductors. *Nat. Comm.* **2023**, *14*, 1343.
- [16] Liu, C.; Palczewski, A. D.; Dhaka, R. S.; Kondo, T.; Fernandes, R. M.; Mun, E. D.; Hodovanets, H.; Thaler, A. N.; Schmalian, J.; Bud'ko, S. L.; Canfield, P. C.; Kaminski, A. Importance of the Fermi-surface topology to the superconducting state of the electron-doped pnictide $\text{Ba}(\text{Fe}_{1-x}\text{Co}_x)_2\text{As}_2$. *Phys. Rev. B* **2011**, *84*, 020509.
- [17] Caivano, R.; Fratini, M.; Poccia, N.; Ricci, A.; Puri, A.; Ren, Z.-A.; Dong, X.-L.; Yang, J.; Lu, W.; Zhao, Z.-X.; others Feshbach resonance and mesoscopic phase separation near a quantum critical point in multiband FeAs-based superconductors. *Supercond. Sci. Technol.* **2008**, *22*, 014004.
- [18] Homeier, L.; Lange, H.; Demler, E.; Bohrdt, A.; Grusdt, F. Feshbach hypothesis of high- T_c superconductivity in cuprates. *Nat. Comm.* **2025**, *16*, 314.
- [19] Joe, Y. S.; Satanin, A. M.; Kim, C. S. Classical analogy of Fano resonances. *Phys. Scr.* **2006**, *74*, 259.
- [20] Fano, U. Effects of Configuration Interaction on Intensities and Phase Shifts. *Phys. Rev.* **1961**, *124*, 1866–1878.
- [21] Feshbach, H. Unified theory of nuclear reactions. *Ann. Phys.* **1958**, *5*, 357–390.
- [22] Chin, C.; Grimm, R.; Julienne, P.; Tiesinga, E. Feshbach resonances in ultracold gases. *Rev. Mod. Phys.* **2010**, *82*, 1225–1286.
- [23] Miroshnichenko, A. E.; Flach, S.; Kivshar, Y. S. Fano resonances in nanoscale structures. *Rev. Mod. Phys.* **2010**, *82*, 2257–2298.
- [24] Bianconi, A. Shape resonances in superstripes. *Nat. Phys.* **2013**, *9*, 536–537.
- [25] Bianconi, A.; Bianconi, G.; Caprara, S.; Di Castro, D.; Oyanagi, H.; Saini, N. L. The stripe criticalpoint for cuprates. *J. Phys.: Condens. Matter.* **2000**, *12*, 10655.
- [26] Innocenti, D.; Poccia, N.; Ricci, A.; Valletta, A.; Caprara, S.; Perali, A.; Bianconi, A. Resonant and crossover phenomena in a multiband superconductor: Tuning the chemical potential near a band edge. *Phys. Rev. B.* **2010**, *82*, 184528.
- [27] Kugel, K.; Rakhmanov, A.; Sboychakov, A.; Poccia, N.; Bianconi, A. Model for phase separation controlled by doping and the internal chemical pressure in different cuprate superconductors. *Phys. Rev. B.* **2008**, *78*, 165124.
- [28] Poccia, N.; Fratini, M. The misfit strain critical point in the 3D phase diagrams of cuprates. *J. Supercond. Nov. Magn.* **2009**, *22*, 299–303.
- [29] Valletta, A.; Bianconi, A.; Perali, A.; Logvenov, G.; Campi, G. High- T_c superconducting dome in artificial heterostructures made of nanoscale quantum building blocks. *Phys. Rev. B* **2024**, *110*, 184510.
- [30] Kiss, T.; Yokoya, T.; Chainani, A.; Shin, S.; Hanaguri, T.; Nohara, M.; Takagi, H. Charge-order-maximized momentum-dependent superconductivity. *Nat. Phys.* **2007**, *3*, 720–725.
- [31] Borisenko, S. V.; Kordyuk, A. A.; Zabolotnyy, V. B.; Inosov, D. S.; Evtushinsky, D.; Büchner, B.; Yaresko, A. N.; Varykhalov, A.; Follath, R.; Eberhardt, W.; Patthey, L.; Berger, H. Two Energy Gaps and Fermi-Surface “Arcs” in NbSe_2 . *Phys. Rev. Lett.* **2009**, *102*, 166402.
- [32] Moulding, O.; Osmond, I.; Flicker, F.; Muramatsu, T.; Friedemann, S. Absence of superconducting dome at the charge-density-wave quantum phase transition in $2H\text{-NbSe}_2$. *Phys. Rev. Res.* **2020**, *2*, 043392.
- [33] Sanna, A.; Pellegrini, C.; Liebhaber, E.; Rosnagel, K.; Franke, K. J.; Gross, E. Real-space anisotropy of the superconducting gap in the charge-density wave material $2H\text{-NbSe}_2$. *npj Quantum Materials* **2022**, *7*, 6.
- [34] Weber, F.; Rosenkranz, S.; Heid, R.; Said, A. H. Superconducting energy gap of $2H\text{-NbSe}_2$ in phonon spectroscopy. *Phys. Rev. B* **2016**, *94*, 140504.
- [35] Feng, L. et al. Dynamical interplay between superconductivity and charge density waves: A nonlinear terahertz study of coherently driven $2H\text{-NbSe}_2$. *Phys. Rev. B* **2023**, *108*, L100504.
- [36] Venturini, R.; Sarkar, A.; Sutar, P.; Jagličić, Z.; Vaskivskyi, Y.; Goresnik, E.; Mihailovic, D.; Mertelj, T. Unconventional photoinduced charge density wave dynamics in $2H\text{-NbSe}_2$. *Phys. Rev. B* **2023**, *108*, 235160.
- [37] Pásztor, Á.; Scarfato, A.; Spera, M.; Flicker, F.; Barreteau, C.; Giannini, E.; Wezel, J. v.; Renner, C. Multiband charge density wave exposed in a transition metal dichalcogenide. *Nat. Comm.* **2021**, *12*, 6037.
- [38] Arguello, C. J.; Chockalingam, S. P.; Rosenthal, E. P.; Zhao, L.; Gutiérrez, C.; Kang, J. H.; Chung, W. C.; Fernandes, R. M.; Jia, S.; Millis, A. J.; Cava, R. J.; Pasupathy, A. N. Visualizing the charge density wave transition in $2H\text{-NbSe}_2$ in real space. *Phys. Rev. B* **2014**, *89*, 235115.

- [39] Soumyanarayanan, A.; Yee, M. M.; He, Y.; Van Wezel, J.; Rahn, D. J.; Rossnagel, K.; Hudson, E.; Norman, M. R.; Hoffman, J. E. Quantum phase transition from triangular to stripe charge order in NbSe₂. *PNAS* **2013**, *110*, 1623–1627.
- [40] Rohwer, T.; Hellmann, S.; Wiesenmayer, M.; Sohr, C.; Stange, A.; Slomski, B.; Carr, A.; Liu, Y.; Avila, L. M.; Kalläne, M.; others Collapse of long-range charge order tracked by time-resolved photoemission at high momenta. *Nature* **2011**, *471*, 490–493.
- [41] Mitrano, M. et al. Ultrafast time-resolved x-ray scattering reveals diffusive charge order dynamics in La_{2-x}Ba_xCuO₄. *Sci. Adv.* **2019**, *5*, eaax3346.
- [42] Leroux, M.; Errea, I.; Le Tacon, M.; Souliou, S.-M.; Garbarino, G.; Cario, L.; Bosak, A.; Mauri, F.; Calandra, M.; Rodière, P. Strong anharmonicity induces quantum melting of charge density wave in 2H-NbSe₂ under pressure. *Phys. Rev. B* **2015**, *92*, 140303.
- [43] Chatterjee, U.; Zhao, J.; Iavarone, M.; Di Capua, R.; Castellán, J.-P.; Karapetrov, G.; Malliakas, C. D.; Kanatzidis, M. G.; Claus, H.; Ruff, J. P.; others Emergence of coherence in the charge-density wave state of 2H-NbSe₂. *Nat. Comm.* **2015**, *6*, 6313.
- [44] Johannes, M. D.; Mazin, I. I. Fermi surface nesting and the origin of charge density waves in metals. *Phys. Rev. B* **2008**, *77*, 165135.
- [45] Flicker, F.; Van Wezel, J. Charge order from orbital-dependent coupling evidenced by NbSe₂. *Nat. Comm.* **2015**, *6*, 7034.
- [46] Cao, L.; Xue, Y.; Wang, Y.; Zhang, F.-C.; Kang, J.; Gao, H.-J.; Mao, J.; Jiang, Y. Directly visualizing nematic superconductivity driven by the pair density wave in NbSe₂. *Nat. Comm.* **2024**, *15*, 7234.
- [47] Lian, C.-S.; Si, C.; Duan, W. Unveiling Charge-Density Wave, Superconductivity, and Their Competitive Nature in Two-Dimensional NbSe₂. *Nano Lett.* **2018**, *18*, 2924–2929, PMID: 29652158.
- [48] He, R.; van Baren, J.; Yan, J.-A.; Xi, X.; Ye, Z.; Ye, G.; Lu, I.-H.; Leong, S. M.; Lui, C. H. Interlayer breathing and shear modes in NbSe₂ atomic layers. *2D Mater.* **2016**, *3*, 031008.
- [49] Tsang, J. C.; Smith, J. E.; Shafer, M. W. Raman Spectroscopy of Soft Modes at the Charge-Density-Wave Phase Transition in 2H-NbSe₂. *Phys. Rev. Lett.* **1976**, *37*, 1407–1410.
- [50] Sooryakumar, R.; Klein, M. V. Raman Scattering by Superconducting-Gap Excitations and Their Coupling to Charge-Density Waves. *Phys. Rev. Lett.* **1980**, *45*, 660–662.
- [51] Méasson, M.-A.; Gallais, Y.; Cazayous, M.; Clair, B.; Rodière, P.; Cario, L.; Sacuto, A. Amplitude Higgs mode in the 2H-NbSe₂ superconductor. *Phys. Rev. B* **2014**, *89*, 060503.
- [52] Du, Y.; Liu, G.; Ruan, W.; Fang, Z.; Watanabe, K.; Taniguchi, T.; Liu, R.; Li, J.-X.; Xi, X. Unveiling Resilient Superconducting Fluctuations in Atomically Thin NbSe₂ through Higgs Mode Spectroscopy. *Phys. Rev. Lett.* **2025**, *134*, 066002.
- [53] Cardona, M. *Light Scattering in Solids I: Introductory Concepts*; Springer Science & Business Media, 2005; Vol. 8.
- [54] Eklund, P. C.; Subbaswamy, K. R. Analysis of Breit-Wigner line shapes in the Raman spectra of graphite intercalation compounds. *Phys. Rev. B* **1979**, *20*, 5157–5161.
- [55] Blumberg, G.; Klein, M.; Börjesson, L.; Liang, R.; Hardy, W. Investigation of the temperature dependence of electron and phonon Raman scattering in single crystal YBa₂Cu₃O_{6.952}. *J. Supercond.* **1994**, *7*, 445–448.
- [56] Sheng, S.; Abdo, M.; Rolf-Pissarczyk, S.; Lichtenberg, K.; Baumann, S.; Burgess, J. A.; Malavolti, L.; Loth, S. Terahertz spectroscopy of collective charge density wave dynamics at the atomic scale. *Nature Physics* **2024**, *20*, 1603–1608.
- [57] Cao, Z.-Y.; Zhang, K.; Goncharov, A. F.; Yang, X.-J.; Xu, Z.-A.; Chen, X.-J. Pressure effect of the charge density wave transition on Raman spectra and transport properties of 2H-NbSe₂. *Phys. Rev. B* **2023**, *107*, 245125.
- [58] Giannetti, C.; Capone, M.; Fausti, D.; Fabrizio, M.; Parmigiani, F.; Mihailovic, D. Ultrafast optical spectroscopy of strongly correlated materials and high-temperature superconductors: a non-equilibrium approach. *Adv. Phys.* **2016**, *65*, 58–238.
- [59] Yusupov, R.; Mertelj, T.; Kabanov, V. V.; Brazovskii, S.; Kusar, P.; Chu, J.-H.; Fisher, I. R.; Mihailovic, D. Coherent dynamics of macroscopic electronic order through a symmetry breaking transition. *Nat. Phys.* **2010**, *6*, 681–684.
- [60] Kabanov, V. V.; Demsar, J.; Podobnik, B.; Mihailovic, D. Quasiparticle relaxation dynamics in superconductors with different gap structures: Theory and experiments on YBa₂Cu₃O_{7-δ}. *Phys. Rev. B* **1999**, *59*, 1497–1506.
- [61] Demsar, J.; Biljaković, K.; Mihailovic, D. Single Particle and Collective Excitations in the One-Dimensional Charge Density Wave Solid K_{0.3}MoO₃ Probed in Real Time by Femtosecond Spectroscopy. *Phys. Rev. Lett.* **1999**, *83*, 800–803.
- [62] Nussinov, Z.; Vekhter, I.; Balatsky, A. V. Nonuniform glassy electronic phases from competing local orders. *Phys. Rev. B* **2009**, *79*, 165122.
- [63] Schmalian, J.; Wolynes, P. G. Stripe Glasses: Self-Generated Randomness in a Uniformly Frustrated System. *Phys. Rev. Lett.* **2000**, *85*, 836–839.
- [64] Ricci, A.; Poccia, N.; Campi, G.; Mishra, S.; Müller, L.; Joseph, B.; Shi, B.; Zozulya, A.; Buchholz, M.; Trabant, C.; others Measurement of spin dynamics in a layered nickelate using X-ray Photon correlation spectroscopy: Evidence for Intrinsic destabilization of Incommensurate stripes at low temperatures. *Phys. Rev. Lett.* **2021**, *127*, 057001.
- [65] Campi, G.; Bianconi, A.; Joseph, B.; Mishra, S. K.; Müller, L.; Zozulya, A.; Nugroho, A. A.; Roy, S.; Sprung, M.; Ricci, A. Nanoscale inhomogeneity of charge density waves dynamics in La_{2-x}Sr_xNiO₄. *Sci. Rep.* **2022**, *12*, 15964.
- [66] Jotzu, G.; Meier, G.; Cantaluppi, A.; Cavalleri, A.; Pontiroli, D.; Riccò, M.; Ardavan, A.; Nam, M.-S. Superconducting Fluctuations Observed Far above T_c in the Isotropic Superconductor K₃C₆₀. *Phys. Rev. X* **2023**, *13*, 021008.
- [67] Sachdev, S.; Starykh, O. A. Thermally fluctuating superconductors in two dimensions. *Nature* **2000**, *405*, 322–325.
- [68] Zullo, L.; Setnikar, G.; Pawbake, A.; Cren, T.; Brun, C.; Cordiez, J.; Sasaki, S.; Cario, L.; Marini, G.; Calandra, M.; Méasson, M.-A. Charge density wave collapse of NbSe₂ in the (LaSe)_{1.14}(NbSe₂)₂ misfit layer compound.

- Phys. Rev. B* **2024**, *110*, 075430.
- [69] Xi, X.; Zhao, L.; Wang, Z.; Berger, H.; Forró, L.; Shan, J.; Mak, K. F. Strongly enhanced charge-density-wave order in monolayer NbSe₂. *Nat. Nanotechnol.* **2015**, *10*, 765–769.
- [70] Anikin, A.; Schaller, R. D.; Wiederrecht, G. P.; Margine, E. R.; Mazin, I. I.; Karapetrov, G. Ultrafast dynamics in the high-symmetry and in the charge density wave phase of 2H-NbSe₂. *Phys. Rev. B* **2020**, *102*, 205139.
- [71] Payne, D. T.; Barone, P.; Benfatto, L.; Parmigiani, F.; Cilento, F. Lattice contribution to the unconventional charge density wave transition in 2H-NbSe₂: a non-equilibrium optical approach. 2020; <https://arxiv.org/abs/2010.09826>.
- [72] Devereaux, T. P.; Hackl, R. Inelastic light scattering from correlated electrons. *Rev. Mod. Phys.* **2007**, *79*, 175–233.
- [73] Klein, M. V. In *Light Scattering in Solids I*; Cardona, M., Ed.; Top. Appl. Phys.; Springer: Berlin, 1983; Vol. 8; pp 147–201.
- [74] Mialitsin, A. Fano line shape and anti-crossing of Raman active E_{2g} peaks in the charge density wave state of NbSe₂. *J. Phys. Chem. Solids* **2011**, *72*, 568–571.
- [75] Eklund, P.; Subbaswamy, K. Analysis of Breit-Wigner line shapes in the Raman spectra of graphite intercalation compounds. *Phys. Rev. B.* **1979**, *20*, 5157.
- [76] Joe, Y. S.; Satanin, A. M.; Kim, C. S. Classical analogy of Fano resonances. *Phys. Scr.* **2006**, *74*, 259–266.